Design and Performance Analysis of a New STBC-MIMO LoRa System

Huan Ma, Guofa Cai, *Member, IEEE*, Yi Fang, *Member, IEEE*, Pingping Chen, *Member, IEEE*, and Guojun Han, *Senior Member, IEEE*

***Abstract*— LoRa is a modulation technology for low power wide area networks (LPWAN) with enormous potential in 5G era. However, the performance of LoRa system deteriorates seriously in fading-channel environments. To tackle this problem, in this paper we introduce multiple-input-multiple-output (MIMO) configuration employing space-time block coding (STBC) schemes into the LoRa system to formulate an STBC-MIMO LoRa system. Then, we investigate the theoretical performance of the proposed system over Rayleigh fading channels. To this end, we derive the distribution of the decision metric for the demodulator in the proposed system. Based on the above distribution, we propose a closed-form approximate BER expression of the proposed system when perfect and imperfect channel state information (CSI) are considered. Furthermore, we analyze the diversity order and the throughput of the proposed system. The results of the diversity analysis demonstrate that the diversity order of the system in the imperfect CSI scenario with fixed channel estimate error variance is zero. However, in the imperfect CSI scenario with a decreasing channel estimate error variance and the perfect CSI scenario, the system can achieve full diversity. In addition, the results of the throughput analysis show that the throughput of the proposed system is little affected by CSI conditions. Simulation results verify the accuracy of the theoretical analysis and the excellent performance of the proposed system. Due to such superiority, the proposed STBC-MIMO LoRa system can be considered as a good scheme for LPWAN.**

***Index Terms*— Internet of Things (IoT), LoRa, bit error rate (BER), space-time block coding (STBC), multiple-input-multiple-output (MIMO), diversity order, Rayleigh fading channel.**

Manuscript received January 23, 2021; revised April 21, 2021; accepted May 27, 2021. Date of publication June 7, 2021; date of current version September 16, 2021. This work was supported in part by the NSF of China (Nos. 62071129, 62071131, 61771149, U2001203, 61871136, 61871132); in part by the Open Research Fund of the State Key Laboratory of Integrated Services Networks under Grant ISN22-23; in part by the NSF of Guangdong Province under Grant 2019A1515011465; in part by the Science and Technology Program of Guangzhou under Grant 201904010124; in part by the Project of Department of Education of Guangdong Province (No. 2021XSLT020, 2018SFJD-01); in part by the Research Project of the Education Department of Guangdong Province under Grant 2018KTSCX057, Grant 2017KTSCX060, and Grant 2017KZDXM028; in part by the Graduate Education and Innovation Project of Guangdong Province under Grant 2020SQXX12; and in part by the Guangdong Innovative Research Team Program under Grant 2014ZT05G157. The associate editor coordinating the review of this article and approving it for publication was M. J. Hossain. *(Corresponding author: Guofa Cai.)*

Huan Ma, Guofa Cai, Yi Fang, and Guojun Han are with the School of Information Engineering, Guangdong University of Technology, Guangzhou 510006, China, and also with the State Key Laboratory of Integrated Services Networks, Xidian University, Xi'an 710126, China (e-mail: mh-zs@163.com; caiguofa2006@126.com; fangyi@gdut.edu.cn; gjhan@gdut.edu.cn).

Pingping Chen is with the Department of Electronic Information, Fuzhou University, Fuzhou 350116, China (e-mail: ppchen.xm@gmail.com).

Color versions of one or more figures in this article are available at https://doi.org/10.1109/TCOMM.2021.3087122.

Digital Object Identifier 10.1109/TCOMM.2021.3087122

I. Introduction

With the continuous update and improvement of Internet of things (IoT) and 5G technologies, massive connectivity has become one of the most important backbones of current world development. By providing real-time information, analysis and decision-making, the IoT in the 5G era is greatly changing the previous business models and lifestyles of people, such as driverless cars, unmanned aerial vehicle, smart appliances, and automated factories, thereby bringing unlimited possibilities for the future development of society. The widely promoted low power wide area network (LPWAN) plays an important role in 5G networks in recent years [1], because it can complement traditional cellular and short-range wireless technologies to address the different requirements of IoT applications. It is estimated that in 2022, the number of compatible nodes for LPWAN will reach 350 million [2].

For LPWAN, several communication technologies have been proposed, such as NB-IoT [3], Sigfox [4], and LoRa [5], [6]. Compared with NB-IoT- and Sigfox-based LPWAN, LoRa-based LPWAN has some unique advantages such as being highly open and flexible. Furthermore, LoRa-based LPWAN can be deployed in a private network and the operating cost of this LPWAN is low. As a modulation scheme of LPWAN, LoRa has gained considerable commercial traction and its specifications are maintained by the LoRa Alliance.[1] LoRa is a low-power, low-speed, and long-range modulation based on chirp spread-spectrum (CSS) technology [7]. In the LoRa modulation, cyclic shifts of chirp signal with linearly increased frequency form a multidimensional space for LoRa symbols, and the signals of different LoRa symbols are orthogonal to each other [8]. The coverage of LoRa is determined by the spreading factor. Increasing the spreading factor can provide wider coverage but reduce the data rate [9].

With the expansion of the market share occupied by LoRa in LPWAN, the number of countries deploying LoRa-based solutions has grown rapidly, which has reached 142 [6]. Accordingly, LoRa has also attracted more and more attention from academia. To explore various performance indicators of the LoRa modulation, researchers have carried out a lot of experimental-based works in the real world. In [10]–[13], the coverage capability of LoRa has been studied. In different scenarios, the coverage of LoRa ranges from 100m to 30km. In [12], the coverage of LoRa in an outdoor scenario has been evaluated by deploying a LoRa base station on a mountain.

[1] https://lora-alliance.org

The results of the study indicate that the LoRa base station at an altitude of 470m can cover an area of 1380 square kilometers. In [13], it has been observed that the available communication distances of LoRa are 15km in the ground environment and 30km in the water environment.

After some pioneering work based on experiments, research on LoRa networks has attracted growing interest. With the increasing density of IoT applications, some work has considered the scalability and capacity of LoRa. In [14], mathematical tools has been utilized to simulate the uplink coverage of the single gateway LoRa network and it reveals the unique physical layer characteristics of the LoRa network. In [15], scalability performance has been conducted on a LoRa network with multiple gateways, and the impact of confirmed and unconfirmed messages on the traffic of a large-scale LoRa network has been analyzed. In addition, theoretical LoRa capacity has been explored in [16]–[18], where ALOHA network model is utilized to characterize LoRa-based LPWAN. In [19], a more practical model considering capture effect has been adopted to analyze LoRa capacity. Moreover, some recent research works have been studied to design multi-hop and multi-relay schemes for improving reliability of LoRa networks, e.g., concurrent transmission multi-hop LoRa network [20], multi-hop LoRa network with tree-based spreading factor clustering algorithm [21], and cooperative LoRa networks [22], [23].

While the LoRa physical layer is protected by patent [24], the study on such a modulation has become more active recently due to the implementation of reverse engineering [25], [26]. A rigorous mathematical description of the LoRa modulation and demodulation process has been developed in [8], and subsequently the waveform and spectral characteristics of the LoRa modulation have been investigated in [27]. In addition, bit-error-rate (BER) performance analysis of the LoRa modulation has been performed in [28], [29]. The analytical results show that the poor performance of the LoRa system might not sustain long-range communication in the fading environment. For this reason, some improved modulation schemes based on the physical layer of LoRa have been proposed, such as phase-shift-keying (PSK) LoRa [30], interleaved chirp spreading LoRa [31], and dual orthogonal LoRa [32]. All of these schemes aim at enhancing the capacity of the LoRa network.

Multiple-input-multiple-output (MIMO) technology is a desirable solution to improve the reliability of wireless communication systems [33]. In particular, by employing space-time block coding (STBC), an MIMO system can be easily realized to achieve considerable transmit and receive diversity over wireless channels. The STBC for two transmit antennas has been first proposed by Alamouti [34], and has subsequently been generalized to the scenario of more than two transmit antennas [35], [36]. On the basis of these schemes, a variety of the enhanced STBCs have been conceived for different application scenarios [37]–[39]. Thanks to the appealing advantages, MIMO technology has been introduced into spread-spectrum communication systems [40]–[43]. More recently, researchers have endeavored to apply such technology to LoRa systems. A LoRa-aided binary PSK MIMO system has been presented in [44]. However, the LoRa signal in this system is only utilized to spread the spectrum of the BPSK baseband signal rather than carrying information, which leads to severe data-rate loss. In [45], a system offering joint localization and range extensions for LPWANs has been proposed. In such a system, MIMO technique is utilized in LoRa end devices and LoRa gateways to achieve a higher signal-to-noise ratio (SNR) with limited additional cost. The experimental results of this system can be found in [46].

With the above motivation, we propose a STBC-MIMO scheme with the LoRa modulation (i.e., STBC-MIMO LoRa system) in this paper. Taking into account the low-complexity requirements for the LoRa system, the Alamouti code in [34] and the STBC in [35], [36] are adopted for designing the proposed STBC-MIMO LoRa system. The contributions of this paper are summarized as follows:

1) An STBC-MIMO LoRa system with M transmit antennas and N receive antennas is put forward. The proposed system can greatly improve BER performance, thereby enhancing the reliability of LoRa networks in fading-channel environments.
2) The theoretical BER performance of the proposed system is carefully analyzed over Rayleigh fading channels. Based on the principle of the STBC-MIMO scheme, the theoretical model of the proposed system is established, then the distribution of the decision metric for the demodulator of the proposed system is derived. According to the above distribution, the closed-form approximate BER expression of the proposed system is presented for both perfect and imperfect channel state information (CSI). In particular, two common channel estimation error models (CEEMs) are considered in the analysis.
3) The asymptotic BER performance is investigated to analyze the diversity order of the proposed system. The results indicate that for the fixed channel estimation error variance, the system reaches zero diversity order, while for the perfect CSI and channel estimation error variance being a decreasing function of average SNR, the system can achieve full diversity $d = MN$. In addition, the throughput of the proposed system is further analyzed.
4) Simulation results not only verify the accuracy of the approximate BER expressions and diversity order analysis of the proposed STBC-MIMO LoRa system, but also demonstrate the superior BER performance. Furthermore, we present some design insight for the proposed STBC-MIMO LoRa system.

The remainder of the paper is organized as follows. In Section II, we provide the detailed descriptions of the LoRa modulation/demodulation process and the proposed STBC-MIMO LoRa system. In Section III, we present the closed-form approximate BER expressions of the proposed system for perfect and imperfect CSIs. We also analyze the diversity order and the throughput of the proposed system in the same Section. In Section IV, we present various simulation results with some discussions. Finally, Section V concludes the paper.

II. System Model

A. LoRa Modulation

LoRa is a frequency shift CSS based modulation scheme. In the LoRa modulation, the frequency of the baseband signal varies linearly in a symbol duration and the bandwidth of the LoRa signal is B_w. There are 2^{SF} chips in each LoRa symbol, where $SF \in \{7, 8, \ldots, 12\}$ is the spreading factor of LoRa [18], [28]. For a LoRa symbol x_o, it can carry SF bits, and assuming that the o^{th} transmitted symbol is $s_o = p \in \{0, 1, \ldots, 2^{SF} - 1\}$. The frequency of x_o varies linearly from the starting frequency $f_s = \frac{B_w \cdot p}{2^{SF}}$ to B_w and then folds to 0, in the remaining symbol duration, the frequency continues to change linearly from 0 to f_s [18]. Specifically, the frequency of each chip increases by $\frac{B_w}{2^{SF}}$. Therefore, the discrete-time baseband signal of the LoRa symbol x_o can be expressed as [18]

$$\begin{aligned} w_o(\kappa T_c) &= \sqrt{E_s}\bar{w}_p(\kappa T_c) \\ &= \sqrt{\frac{E_s}{2^{SF}}} \exp\left[j2\pi \left(\frac{\left((p+\kappa) \bmod 2^{SF}\right)^2}{2^{SF+1}} \right) \right], \end{aligned} \quad (1)$$

where $T_c = \frac{1}{B_w}$ is the sample interval, κ denotes the index of the sample at time κT_c, E_s is the symbol energy, and $\bar{w}_p(\kappa T_c)$ is the basis function of $w_o(\kappa T_c)$. As seen from Eq. (1), the LoRa signal transmitting the symbol p can be considered as a cyclic shift of pT_c for the basis CSS signal [18], [28].[2] Since chirp signals with different offsets are mutually orthogonal, for the LoRa signal of the symbol s_o, when it correlates with 2^{SF} possible LoRa signals, it has the following properties [28]

$$\Lambda_i = \sum_{\kappa=0}^{2^{SF}-1} w_o(\kappa T_c) \cdot \bar{w}_i^*(\kappa T_c) = \begin{cases} \sqrt{E_s}, & i = p \\ 0, & i \neq p \end{cases}, \quad (2)$$

where $0 \leq i \leq 2^{SF} - 1$ and $*$ is the complex conjugate operation. The demodulation of the LoRa signal can be performed based on the above properties. For a received signal $r_o(\kappa T_c)$ of the LoRa symbol x_o after transmission over a frequency-flat and time-invariant channel, the output of the correlator in the LoRa demodulator is written as [28]

$$\begin{aligned} \dot{\Lambda}_i &= \sum_{\kappa=0}^{2^{SF}-1} r_o(\kappa T_c) \cdot \bar{w}_i^*(\kappa T_c) \\ &= \sum_{\kappa=0}^{2^{SF}-1} \left(\sqrt{h_c} w_o(\kappa T_c) + w_n(\kappa T_c) \right) \cdot \bar{w}_i^*(\kappa T_c) \\ &= \begin{cases} \sqrt{h_c E_s} + w_{n,i}, & i = p \\ w_{n,i}, & i \neq p \end{cases}, \end{aligned} \quad (3)$$

where $\sqrt{h_c}$ is the magnitude of fading channel coefficient [28], [30], $w_n(\kappa T_c)$ is the complex additive white Gaussian noise (AWGN), and $w_{n,i}$ is the corresponding complex Gaussian noise process [31]. Hence, the symbol s_o can be estimated as

$$\hat{s}_o = \arg \max_{i=0,\ldots,2^{SF}-1} \left(\left| \dot{\Lambda}_i \right| \right), \quad (4)$$

where $|\cdot|$ denotes absolute operation. In addition, another equivalent low complexity method can also be utilized for demodulation. First, the received signal is multiplied with downchirp $\bar{w}_{down}(\kappa T_c)$ (this step is called a *dechirping*) [18], where $\bar{w}_{down}(\kappa T_c)$ can be expressed as

$$\bar{w}_{down}(\kappa T_c) = \sqrt{\frac{1}{2^{SF}}} \exp\left(-j2\pi \frac{\kappa^2}{2^{SF+1}} \right). \quad (5)$$

Afterwards, the 2^{SF} – point discrete Fourier transform (DFT) is performed on the dechirped signal, thus one can obtain as

$$\dot{\mathbf{\Lambda}}_F = \text{DFT}\left(\mathbf{r}_o \odot \bar{\mathbf{w}}_{down} \right), \quad (6)$$

where $\dot{\mathbf{\Lambda}}_F = \left[\dot{\Lambda}_{F,0}, \ldots \dot{\Lambda}_{F,i}, \ldots \dot{\Lambda}_{F,2^{SF}-1} \right]$, $\mathbf{r}_o = \left[r_o(0), r_o(T_c), \ldots, r_o\left((2^{SF}-1)T_c\right) \right]$, $\bar{\mathbf{w}}_{down} = \left[\bar{w}_{down}(0), \bar{w}_{down}(T_c), \ldots, \bar{w}_{down}\left(\left(2^{SF}-1\right)T_c\right) \right]$, and $\odot$ is the Hadamard product operator [47]. Next, the LoRa symbol is estimated by selecting the index of the frequency bin with the maximum magnitude, given by

$$\hat{s}_o = \arg \max_{i=0,\ldots,2^{SF}-1} \left(\left| \dot{\Lambda}_{F,i} \right| \right). \quad (7)$$

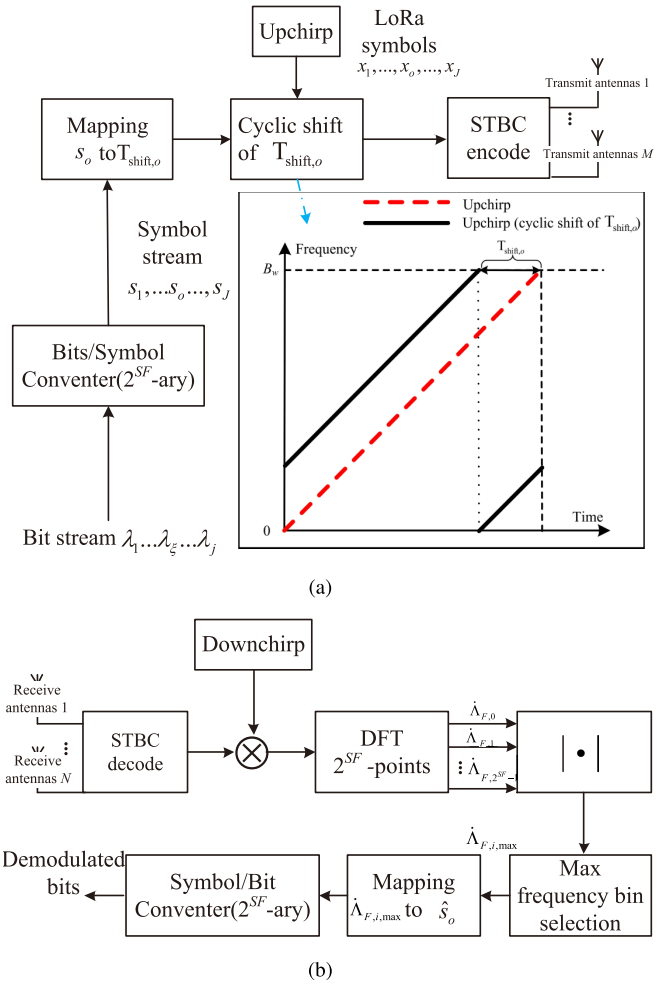

Fig. 1. Illustration of one possible realization of (a) transmitter and (b) receiver for the proposed STBC-MIMO LoRa system.

B. The Proposed STBC-MIMO LoRa System

In this paper, we consider a wireless MIMO system with M ($M \geqslant 2$) transmit antennas and N receive antennas that operates over a flat and quasi-static Rayleigh fading

[2]The basic CSS signal can also be called as the *upchirp* signal, and its frequency varies linearly from 0 to B_w in a symbol duration.

channel,[3] therefore the path gains remain constant in a frame of J symbols and varies from a frame to another [50], [51]. We represent the MIMO channel as an $M \times N$ matrix, $\mathbf{H} = \{h_{m,n}\}$, where $h_{m,n}$ denotes the complex channel gain from the m^{th} transmit antenna to the n^{th} receive antenna. $h_{m,n}$ are independent random variables that follow complex Gaussian distribution with zero mean and variance 0.5 per dimension. Fig. 1 illustrates one possible realization on the transmitter and receiver of the proposed STBC-MIMO LoRa system. In order to be compatible with the LoRa MAC protocol [52], the proposed STBC-MIMO LoRa system utilizes the preamble in the LoRa packet for channel estimation. Here we take the STBC-MIMO LoRa system with two transmitting antennas and two receiving antennas as an example to introduce. It is worth noting that the channel estimator is in the STBC decoder structure. The transmitter first sends L_p preambles through the transmit antenna 1, and the receiver obtains $\hat{h}_{1,1}$ and $\hat{h}_{1,2}$ by the channel estimator. Then, the transmitter sends L_p preambles through the transmit antenna 2, and the receiver obtains $\hat{h}_{2,1}$ and $\hat{h}_{2,2}$ by the channel estimator.

A complex orthogonal STBC transmission matrix $\mathbf{G}$ is represented by a $U \times M$ transmission matrix, where the entries are linear combinations of transmitted symbols $g_1, g_2, \ldots, g_J$ and their conjugates. Moreover, matrix $\mathbf{G}$ satisfies complex orthogonality $\mathbf{G}^H\mathbf{G} = u_{cons}\left(|g_1|^2 + \ldots + |g_J|^2\right)\mathbf{I}_M$ [36], [53], where $\mathbf{I}_M$ is an $M \times M$ identity matrix and u_{cons} is a constant that depends on the STBC transmission matrix [54]. Matrix $\mathbf{G}$ is utilized to encode J $(J \geqslant 2)$ input symbols into an M-dimensional vector sequence of U time slots (i.e., to control the symbol transmission of M transmitting antennas in each slot). Consequently, the transmission rate of STBC is $r = J/U$.

In this paper, the channel estimation matrix at the receiver is modeled as [55]–[57]

$$\hat{\mathbf{H}} = \mathbf{H} + \mathbf{E}_h, \tag{8}$$

where $\mathbf{E}_h = \{e_{m,n}\}$ is an $M \times N$ error matrix independent of $\mathbf{H}$, $e_{m,n}$ are complex Gaussian independent random variables with zero mean and variance σ_e^2, where σ_e^2 reflects the accuracy of the channel estimation. Accordingly, the variance of the estimated channel gain is $\sigma_{\hat{h}}^2 = \sigma_h^2 + \sigma_e^2$. In particular, when $\sigma_e^2 = 0$, it can be considered that perfect channel estimation is performed at the receiver (i.e., the receiver knows perfect CSI). In this paper, two types of channel estimation error variance are considered: one is that σ_e^2 is fixed and independent of the average SNR, and the other is that σ_e^2 is a decreasing function of the average SNR. These two types of error variance correspond to CEEMs I and II, respectively. For the proposed STBC-MIMO LoRa system, when the channel estimation error occurs at the receiver, it causes inter-antenna interference (IAI). Here, we take the STBC $\mathbf{G}_2$ in [58] as an example and apply it to an STBC-MIMO LoRa system with two receive antennas to illustrate the encoding/decoding process in the proposed system. Code $\mathbf{G}_2$ is given by [34]

$$\mathbf{G}_2 = \begin{pmatrix} g_1 & g_2 \\ -g_2^* & g_1^* \end{pmatrix}. \tag{9}$$

Utilizing $\mathbf{G}_2$, we can encode the LoRa symbol in space and time. Taking the encoding of the first two LoRa symbols x_1 (the symbol transmitted by x_1 is $s_1 = p$) and x_2 (the symbol transmitted by x_2 is $s_2 \neq p$) in the sequence as an example, this process is shown in Table I. Correspondingly, the notation for the received signal at the two receive antennas is defined in Table II, where

$$\begin{aligned} r_1 &= h_{1,1}x_1 + h_{2,1}x_2 + n_1 \\ r_2 &= -h_{1,1}x_2^* + h_{2,1}x_1^* + n_2 \\ r_3 &= h_{1,2}x_1 + h_{2,2}x_2 + n_3 \\ r_4 &= -h_{1,2}x_2^* + h_{2,2}x_1^* + n_4, \end{aligned} \tag{10}$$

and n_1, n_2, n_3, and n_4 are the complex AWGN with variance $N_0/2$ per dimension. Next, the maximum likelihood decoding of the STBC can be achieved by linear processing [58] in the STBC decoder at the receiver, thereby recovering the desired LoRa symbols. Without loss of generality, we take x_1 as an example for illustration and following analysis. For the LoRa symbol x_1, the other LoRa symbol x_2 (i.e., the transmitted symbol carried by x_2 is not equal to p) can be regarded as interference. After STBC decoding, the recovered LoRa symbol $\tilde{x}_1$ can be expressed as

$$\begin{aligned} \tilde{x}_1 &= \hat{h}_{1,1}^* r_1 + \hat{h}_{2,1} r_2^* + \hat{h}_{1,2}^* r_3 + \hat{h}_{2,2} r_4^* \\ &= \underbrace{\left(\left|\hat{h}_{1,1}\right|^2 + \left|\hat{h}_{2,1}\right|^2 + \left|\hat{h}_{1,2}\right|^2 + \left|\hat{h}_{2,2}\right|^2 - \hat{h}_{1,1}^* e_{1,1} - \hat{h}_{2,1}^* e_{2,1} - \hat{h}_{1,2} e_{1,2}^* - \hat{h}_{2,2} e_{2,2}^*\right) x_1}_{S_\alpha} \\ &\quad + \underbrace{\left(-\hat{h}_{1,1}^* e_{2,1} + \hat{h}_{2,1} e_{1,1}^* - \hat{h}_{1,2}^* e_{2,2} + \hat{h}_{2,2} e_{2,1}^*\right) x_2}_{S_\beta} \\ &\quad + \underbrace{\left(\hat{h}_{1,1}^* n_1 + \hat{h}_{2,1} n_2^* + \hat{h}_{1,2}^* n_3 + \hat{h}_{2,2} n_4^*\right)}_{S_\tau}, \end{aligned} \tag{11}$$

TABLE I

THE ENCODING AND TRANSMISSION SEQUENCE FOR THE PROPOSED STBC-MIMO LoRa SYSTEM WITH TWO TRANSIT ANTENNAS

	Transmit antenna 1	Transmit antenna 2
Time t_s	x_1	x_2
Time $t_s + 2^{SF}T_c$	$-x_2^*$	x_1^*

TABLE II

THE NOTATION FOR THE RECEIVED SIGNAL AT THE TWO RECEIVE ANTENNAS

	Receive antenna 1	Receive antenna 2
Time t_s	r_1	r_3
Time $t_s + 2^{SF}T_c$	r_2	r_4

[3]The proposed system can be applied for uplink and downlink transmission. Generally, in a MIMO IoT network, the base station is equipped with multiple antennas, while the IoT nodes are equipped with fewer or even one antenna [45], [48], [49]. For general analysis, a wireless system with M transmit antennas and N receive antennas is considered in this paper.

where terms S_α, S_β, and S_τ are the desired signal, IAI and noise, respectively.[4] Accordingly, referring to Eq. (3) and Eq. (4), the decision metric of $\tilde{x}_1$ can be expressed as

$$Z_{\tilde{x}_1,i} = \left| \sum_{\kappa=0}^{2^{SF}-1} w_{\tilde{x}_1}(\kappa T_c) \cdot \bar{w}_i^*(\kappa T_c) \right| = \begin{cases} \left| \begin{array}{l} \sqrt{\frac{E_s}{2}} \left(\left|\hat{h}_{1,1}\right|^2 + \left|\hat{h}_{2,1}\right|^2 \right. \\ \quad + \left|\hat{h}_{1,2}\right|^2 + \left|\hat{h}_{2,2}\right|^2 \\ \quad -\hat{h}_{1,1}^* e_{1,1} + \hat{h}_{2,1} e_{2,1}^* \\ \left. -\hat{h}_{1,2}^* e_{1,2} + \hat{h}_{2,2} e_{2,2}^* \right) \\ \quad +\hat{h}_{1,1}^* \phi_1 + \hat{h}_{2,1} \phi_2^* \\ \quad +\hat{h}_{1,2}^* \phi_3 + \hat{h}_{2,2} \phi_4^* \end{array} \right|, & i = p \\ \left| \begin{array}{l} \sqrt{\frac{E_s}{2}} \left(-\hat{h}_{1,1}^* e_{2,1} + \hat{h}_{2,1} e_{1,1}^* \right. \\ \left. -\hat{h}_{1,2}^* e_{2,2} + \hat{h}_{2,2} e_{1,2}^* \right) + \hat{h}_{1,1}^* \phi_1 \\ \quad +\hat{h}_{2,1} \phi_2^* + \hat{h}_{1,2}^* \phi_3 + \hat{h}_{2,2} \phi_4^* \end{array} \right|, & i \neq p, i = s_2 \\ \left| \begin{array}{l} \hat{h}_{1,1}^* \phi_1 + \hat{h}_{2,1} \phi_2^* \\ + \hat{h}_{1,2}^* \phi_3 + \hat{h}_{2,2} \phi_4^* \end{array} \right| & i \neq p, i \neq s_2 \end{cases}, \tag{12}$$

where $\phi_\wp (\wp = 1, 2, 3, 4)$ is the complex Gaussian noise process caused by $n_\wp$ and $w_{\tilde{x}_1}(\kappa T_c)$ is the discrete-time baseband signal of $\tilde{x}_1$. Then, the symbol s_1 is estimated by

$$\hat{s}_1 = \arg \max_{i=0,\ldots,2^{SF}-1} \left(Z_{\tilde{x}_1,i} \right). \tag{13}$$

More generally, the encoding and decoding algorithms for the STBC-MIMO LoRa system are summarized in Algorithm 1 and Algorithm 2, respectively.

Algorithm 1 Encoding algorithm for the STBC-MIMO LoRa system

Initialization:

Initialize the number of transmit antennas M, spreading factor SF;
Input the transmitted bit streams $\boldsymbol{\lambda}_1, \ldots \boldsymbol{\lambda}_j$;
Bit/symbol converter: $\boldsymbol{\lambda}_1, \ldots \boldsymbol{\lambda}_j \rightarrow s_1, \ldots s_J$.

LoRa modulation:

The transmitted symbols $s_1, \ldots s_J \rightarrow$ LoRa symbols $x_1, \ldots x_J$ (Utilizing Eq. (1)).

STBC-aided encoding:

Choose a $\mathbf{G}_M$ for STBC;
Initialize an $U \times \left(M \cdot 2^{SF}\right)$ zero matrix $\mathfrak{S}$;
By utilizing $\mathbf{G}_M$, obtain the matrix $\mathfrak{S}$ with entries linear combinations of $x_1, \ldots x_J$ and their conjugates;
for $u = 1:1:U$ **do**
  for $\theta = 1:1:M$ **do**
    In the time slot u, the signals in the u^{th} row, $\left[(\theta-1) \cdot 2^{SF} + 1\right]^{th}$ column to $\left(\theta \cdot 2^{SF}\right)^{th}$ column in $\mathfrak{S}$ are transmitted through the θ^{th} antenna.
  end for
end for

Algorithm 2 Decoding algorithm for the STBC-MIMO LoRa system

Initialization:

Initialize the number of transmit antennas N, spreading factor SF, and the signal $\Re_{u,n_t}$ received by the n_t^{th} $(1 \leq n_t \leq N)$ receive antenna in the u^{th} time slot;
Utilize the channel estimator to get the estimated channel gain $\hat{\mathbf{H}}$.

STBC-aided decoding

for $N_{sym} = 1:1:J$ **do**
  $\boldsymbol{z}_{sym,N_{sym}} = [0, \ldots, 0]_{1 \times 2^{SF}}$;
  $\boldsymbol{z}_{N\_temp} = [0, \ldots, 0]_{1 \times 2^{SF}}$;
  for $n_t = 1:1:N$ **do**
    $\boldsymbol{z}_{slot,N_{sym}} = [0, \ldots, 0]_{1 \times 2^{SF}}$;
    for $u = 1:1:U$ **do**
      According to $\mathbf{G}_M$, $\Re_{u,n_t}$ is processed with $\hat{\mathbf{H}}$ (linear processing or conjugate operation) to obtain $\tilde{\Re}_{u,n_t}$;
      $\boldsymbol{z}_{slot\_temp} = \boldsymbol{z}_{slot\_temp} + \tilde{\Re}_{u,n_t}$;
    end for
    $\boldsymbol{z}_{N\_temp} = \boldsymbol{z}_{N\_temp} + \boldsymbol{z}_{slot\_temp}$;
  end for
  $\tilde{\boldsymbol{z}}_{sym,N_{sym}} = \boldsymbol{z}_{N\_temp}$;
end for

LoRa demodulation:

$\tilde{\boldsymbol{z}}_{sym,1}, \ldots, \tilde{\boldsymbol{z}}_{sym,J} \rightarrow \hat{s}_1, \ldots, \hat{s}_J$ (Utilizing Eqs. (6) and (7)).
Symbol/bit converter: $\hat{s}_1, \ldots, \hat{s}_J \rightarrow \hat{\boldsymbol{\lambda}}_1, \ldots \hat{\boldsymbol{\lambda}}_j$.

C. Complexity Analysis

Here, we analyze the complexity of the proposed STBC-MIMO LoRa system. The main computational complexity of the proposed system comes from the channel estimation, STBC decoding and LoRa demodulation.[5] Due to the low-power consumption and low-complexity requirements of LoRa devices, the least-squre method [60] is considered in the channel estimator of the proposed system. The complexities of channel estimation and STBC decoding of the proposed STBC-MIMO LoRa system are $\mathcal{O}(MNL_p\Psi)$ and $\mathcal{O}(JUN\Psi)$, respectively. Where $\Psi = 2^{SF}$. The computational complexity of LoRa demodulation consists of four parts, i.e., dechirping $\mathcal{O}(J\Psi)$, J times DFT $\mathcal{O}\left(J\Psi^2\right)$, performing absolute value operation on the result of DFT $\mathcal{O}(J\Psi)$, and argmax operation $\mathcal{O}(J\Psi)$. Therefore, the total computational complexity of the proposed STBC-MIMO LoRa system is required at an order of $\mathcal{O}\left(\Psi^2\right)$. Notably, the computational complexity of the single-input single-output (SISO) LoRa system to transmit J information bits is $\mathcal{O}\left(J\Psi^2\right) + 3\mathcal{O}(J\Psi)$, which has the same order of computational complexity as the STBC-MIMO LoRa system. For the hardware complexity, like other IoT devices with multiple antennas [45], [48], [49], each

[4]Unlike the conventional-modulation-based (e.g., $\mathcal{M}$-PSK and $\mathcal{M}$-QAM-based) STBC-MIMO systems, the IAI can be regarded as noise [54], [59]. However, in the STBC-MIMO LoRa system, IAI is the signal of the undesired symbol.

[5]Since the STBC encoding of the LoRa symbols in the transmitter only needs to perform linear processing [36] on the LoRa symbols, the computational complexity in the transmitter is very low.

transmit and receive antenna needs to be equipped with a radio frequency chain.

Remark 1: Similar to the LoRa system in [45], the proposed STBC-MIMO LoRa system also requires channel estimation. Nevertheless, the LoRa packet structure in the proposed system does not need to be adjusted, hence the commonly utilized LoRa MAC protocol [52] can still be applied. In the conventional LoRa system, the preamble symbols in the LoRa packet are utilized for synchronization, while in the proposed STBC-MIMO LoRa system, the preamble symbols are utilized not only for synchronization, but also for channel estimation. Moreover, due to the low-power consumption and low-complexity requirements of LoRa devices, the least-square estimator [60] is considered in the proposed system. Although the proposed STBC-MIMO LoRa system introduces additional but limited computational complexity and hardware complexity, it can be observed from the results in Sect. IV that the proposed STBC-MIMO LoRa system has superior BER performance compared to SISO LoRa in fading-channel environments.

III. Performance Analysis

In this section, the average BER expression of the proposed STBC-MIMO LoRa system is derived, then we analyze the throughput of the proposed system. We denote $f_{Ray}(y;\sigma_y)$ and $f_{Ri}(y;m_y,\sigma_y)$ as the probability density functions (PDFs) of the Rayleigh and Rice distributions, respectively, and we denote the cumulative distribution function (CDF) of Rayleigh distribution by $F_{Ray}(y;\sigma_y)$, where m_y and σ_y are the scale and location parameters of the variable y [61]. One can generalize from Eq. (12) that the distribution of the decision metric of x_1 for an STBC-MIMO LoRa system with M transmit antennas and N receive antennas

$$Z_{\tilde{x}_1,i} \sim \begin{cases} f_{Ri}\left(\alpha; ||\hat{\mathbf{H}}||_F^2\sqrt{\frac{E_s}{r^2M}}, \sqrt{\frac{||\hat{\mathbf{H}}||_F^2}{2}\left(\frac{\sigma_e^2E_s}{r^2M}+\frac{N_0}{r}\right)}\right), & i=p \\ f_{Ray}\left(\beta; \sqrt{\frac{||\hat{\mathbf{H}}||_F^2}{2}\left(\frac{\sigma_e^2E_s}{r^2M}+\frac{N_0}{r}\right)}\right), & i\neq p,\ i=s_2,\ldots,s_J \\ f_{Ray}\left(\tau; \sqrt{\frac{||\hat{\mathbf{H}}||_F^2N_0}{2r}}\right), & i\neq p, s_2,\ldots,s_J \end{cases}, \tag{14}$$

where $||\hat{\mathbf{H}}||_F^2 = \sum_{m=1}^{M}\sum_{n=1}^{N}\left|\hat{h}_{m,n}\right|^2$ is the square of the Frobenius norm of $\left\{\hat{h}_{m,n}\right\}$. For convenience, we denote $||\hat{\mathbf{H}}||_F^2$ by X. For a Rayleigh fading channel, X follows a chi-square distribution with MN degrees of freedom. Thus, the average BER of the proposed system can be expressed as

$$\begin{aligned} P_b &= \frac{2^{SF-1}}{2^{SF}-1}\Pr\left[\max_{i,i\neq p}\left(Z_{\tilde{x}_1,i}\right) > Z_{\tilde{x}_1,p}\right] \\ &= \frac{2^{SF-1}}{2^{SF}-1}\int_0^\infty\left[1-\Pr\left[Z_{\tilde{x}_1,p|X} > \max_{i,i\neq p}\left(Z_{\tilde{x}_1,i|X}\right)\right]\right] \\ &\quad \times f_X(X)\,dX \\ &= \frac{2^{SF-1}}{2^{SF}-1}\int_0^\infty\int_0^\infty\Big[1-\left[F_{Ray}(\alpha|X;\sigma_\beta)\right]^{J-1} \\ &\quad \times\left[F_{Ray}(\alpha|X;\sigma_\tau)\right]^{2^{SF}-J}\Big]\times f_{Ri}(\alpha|X;m_\alpha,\sigma_\alpha) \\ &\quad \times f_X(X)\,d\alpha dX, \end{aligned} \tag{15}$$

where $f_X(X)$ is the PDF of X. To simplify Eq. (15), another equivalent form is utilized to represent P_b [18], [62], in which the error probability is expressed in terms of the noise-driven probability and the IAI-driven probability, i.e.,

$$P_b = \frac{2^{SF-1}}{2^{SF}-1}\left[P_{err}^{N} + \left(1-P_{err}^{N}\right)\times P_{err}^{IAI}\right], \tag{16}$$

where

$$\begin{aligned} P_{err}^{N} &= \int_0^\infty\left[1-\Pr\left[Z_{\tilde{x}_1,p|X} > \max_{i,i\neq p,s_2,\ldots,s_J}\left(Z_{\tilde{x}_1,i|X}\right)\right]\right] \\ &\quad \times f_X(X)\,dX \\ &= \int_0^\infty\int_0^\infty\left[1-\left[F_{Ray}(\alpha|X;\sigma_\tau)\right]^{2^{SF}-J}\right] \\ &\quad \times f_{Ri}(\alpha;m_\alpha,\sigma_\alpha)\times f_X(X)\,d\alpha dX, \end{aligned} \tag{17}$$

$$\begin{aligned} P_{err}^{IAI} &= \int_0^\infty\left[1-\Pr\left[Z_{\tilde{x}_1,p|X} > \max_{i,i\neq p,i=s_2,\ldots,s_J}\left(Z_{\tilde{x}_1,i|X}\right)\right]\right] \\ &\quad \times f_X(X)\,dX \\ &= \int_0^\infty\int_0^\infty\left[1-\left[F_{Ray}(\alpha|X;\sigma_\beta)\right]^{J-1}\right] \\ &\quad \times f_{Ri}(\alpha;m_\alpha,\sigma_\alpha)\times f_X(X)\,dXd\alpha. \end{aligned} \tag{18}$$

In Eqs. (17) and (18), because $f_{Ri}(\alpha|X;m_\alpha,\sigma_\alpha)$ in the integrand contains a modified Bessel function [63], the overflow and accuracy problems will be faced when the numerical calculation is performed. Considering that when the Rice factor K is large, the Rice distribution can be well approximated as a Gaussian distribution [61], thus the Rice factor K_α of $f_{Ri}(\alpha|X;m_\alpha,\sigma_\alpha)$ is further analyzed, which can be expressed as

$$K_\alpha = \frac{m_\alpha^2}{2\sigma_\alpha^2} = \frac{X\cdot \mathrm{T}\cdot 2^{SF}}{(\sigma_e^2\cdot \mathrm{T}\cdot 2^{SF}+rM)}, \tag{19}$$

where $\mathrm{T} = E_s/(N_0\cdot 2^{SF})$ is the SNR in the LoRa communication [28]. It can be observed from Eq. (19) that since X is a random variable, K_α is also a random variable related to X. Fig. 2 shows the PDF of K_α by Monte Carlo simulation under different parameters (e.g., r, M, N, SF, T, and σ_e^2), where $\sigma_e^2 = 0$ and $\sigma_e^2 \neq 0$ correspond to the perfect CSI and the imperfect CSI scenarios, respectively, where L_p denotes the number of the preamble symbol utilized for channel estimation. When σ_e^2 is nonzero and fixed, it corresponds to CEEM I, while when $\sigma_e^2 = 1/(1+L_p\mathrm{T}_{eff})$, it corresponds to CEEM II [59], [64].[6] It can be seen that K_α is basically distributed in the region of $K_\alpha \geq 10\mathrm{dB}$ in both perfect CSI and imperfect CSI scenarios. Hence, the Rice random variable α approximately follows a Gaussian distribution $\mathcal{N}\left(m_\alpha,\sigma_\alpha^2\right)$ [61]. However, in the imperfect CSI scenario with CEEM I, it can be observed from Figs. 2(c) and 2(d) that K_α hardly increases with the increase of SNR in high SNR region. Therefore, considering that in presence of

[6] $\mathrm{T}_{eff} = 2^{SF}\cdot\mathrm{T}$ is the effective SNR for the target symbol [28].

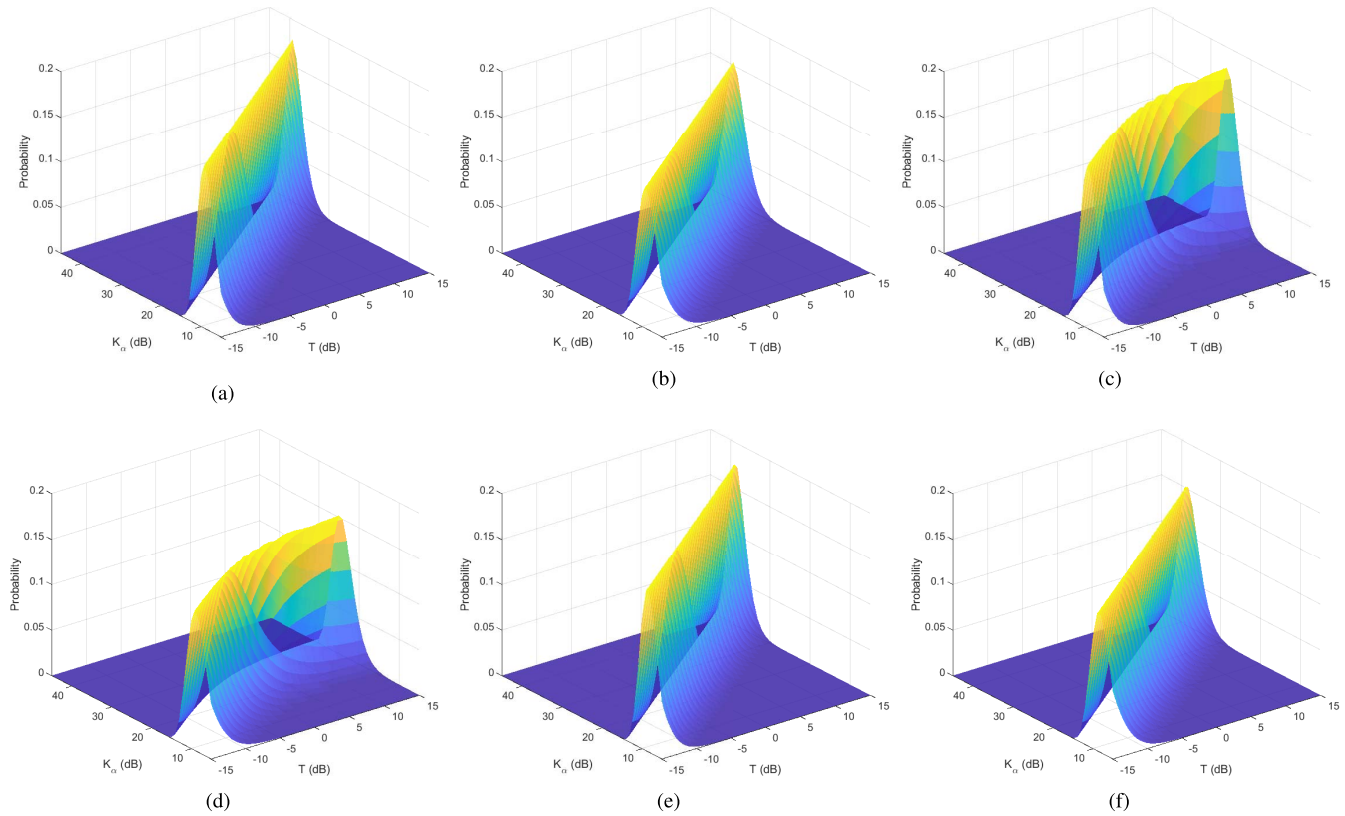

Fig. 2. The PDF of K_α versus SNR with parameters $\{r, M, N, SF, \sigma_e^2\}$ = (a) $\{1, 2, 2, 7, 0\}$, (b) $\{0.5, 3, 1, 7, 0\}$, (c) $\{1, 2, 2, 7, 0.01\}$, (d) $\{0.5, 3, 1, 7, 0.01\}$, (e) $\{1, 2, 2, 7, 1/(1 + L_p \mathrm{T}_{eff})\}$, (f) $\{0.5, 3, 1, 7, 1/(1 + L_p \mathrm{T}_{eff})\}$, where L_p is set to 4.

imperfect CSI, P_b in high SNR region is dominated by P_{err}^{IAI}, the Gaussian distribution will not be utilized to approximate the Rice distribution in the derivation of P_{err}^{IAI} in order to ensure the accuracy of the performance analysis in high SNR region (although this phenomenon does not occur under the CEEM II, for consistency of the derivation of P_{err}^{IAI} under the CEEM I and the CEEM II, the Gaussian distribution will not be utilized to approximate the Rice distribution in the entire derivation of P_{err}^{IAI}).

In addition to the above numerical problems, since SF can be up to 12, $[F_{Ray}(\alpha|X;\sigma_J)]^{2^{SF}-1}$ in Eq. (17) has a very high complexity. Here, let $\tau_{\max} = \max_{i,i\neq p,s_2,\ldots,s_J}(Z_{\tilde{x}_1,i})$, and then refer to the procedure in [28] to approximate the distribution of variable $\tau_{\max}$ by a Gaussian distribution $\mathcal{N}(\mu_{\tau_{\max}}, \sigma_{\tau_{\max}}^2)$. Specifically, $\mu_{\tau_{\max}}$ and $\sigma_{\tau_{\max}}^2$ are respectively given by

$$\mu_{\tau_{\max}} = \left[X^2\left(\frac{N_0^2 \cdot \hbar_{2^{SF}-J}^2}{r^2} - \frac{N_0^2 \cdot \lambda_{2^{SF}-J}}{2r^2}\right)\right]^{\frac{1}{4}}, \quad (20)$$

$$\sigma_{\tau_{\max}}^2 = \frac{X^2}{r}\left(N_0\hbar_{2^{SF}-J} - \sqrt{N_0^2\hbar_{2^{SF}-J}^2 - \frac{N_0^2\lambda_{2^{SF}-J}}{2}}\right), \quad (21)$$

where $\hbar_k = \sum_{q=1}^{k} \frac{1}{q}$ denotes the k^{th} harmonic number and $\lambda_k = \sum_{q=1}^{k} \frac{1}{q^2}$.

Based on the above approximation of the distribution of the random variables α and $\tau_{\max}$, P_{err}^N can be approximated as

$$\begin{aligned} P_{err}^N &\approx \int_0^\infty Q\left(\frac{\mu_\alpha - \mu_{\tau_{\max}}}{\sqrt{\sigma_\alpha^2 + \sigma_{\tau_{\max}}^2}}\right) \cdot f_X(X)\, dX \\ &= \int_0^\infty Q\left(\left(\sqrt{\frac{X^2 E_s}{N_0 r M}} - \left(\hbar_{2^{SF}-J}^2 - \frac{\lambda_{2^{SF}-J}}{2}\right)^{\frac{1}{4}}\right)\right. \\ &\quad \left.\div\sqrt{\left(\frac{\sigma_e^2 E_s}{2N_0 r M} + \frac{1}{2}\right) + \hbar_{2^{SF}-J} - \sqrt{\hbar_{2^{SF}-J}^2 - \frac{\lambda_{2^{SF}-J}}{2}}}\right) \\ &\quad \times f_X(X)\, dX, \end{aligned} \quad (22)$$

where $Q(\cdot)$ is the Q-function [65], [66]. Since $SF \in \{7, \ldots, 12\}$, $\hbar_{2^{SF}-J} \gg \frac{\lambda_{2^{SF}-J}}{2}$. Hence, one can obtain

$$P_{err}^N \approx \int_0^\infty Q\left(\frac{A\sqrt{X} - B}{C}\right) \cdot DX^{MN-1} \cdot e^{-EX} dX, \quad (23)$$

where $A = \sqrt{\frac{\mathrm{T}\cdot 2^{SF}}{rM}}$, $B = \sqrt{\hbar_{2^{SF}-J}}$, $C = \sqrt{\frac{\sigma_e^2 \mathrm{T}\cdot 2^{SF}}{2rM} + \frac{1}{2}}$, $D = \frac{1}{\Gamma(MN)\cdot(1+\sigma_e^2)^{MN}}$, $\Gamma(\cdot)$ denotes Gamma function [63], and $E = -\frac{1}{1+\sigma_e^2}$. Next, further derivations of P_{err}^N and P_{err}^{IAI} are performed in the perfect CSI and the imperfect CSI scenarios.

A. Perfect CSI

Since there is no IAI in the perfect CSI scenario, the BER of the proposed STBC-MIMO LoRa system only depends on the

noise-driven error probability in this scenario. In order to evaluate Eq. (23), we need to approximate the Q-function. According to the relationship between the Gaussian Q-function and the complementary error function $\mathrm{erfc}(\cdot)$, given by [67]

$$Q(x) = \frac{1}{2}\mathrm{erfc}\left(\frac{x}{2}\right), \tag{24}$$

when $\sigma_e^2 = 0$, Eq. (23) can be rewritten as

$$P_{err}^{N} \approx \frac{1}{2}D\int_0^{\infty} \mathrm{erfc}\left(A\sqrt{X} - B\right) \cdot X^{MN-1}e^{-X}dX. \tag{25}$$

According to [68], we can approximate $\mathrm{erfc}(y)$ quite well by utilizing

$$\mathrm{erfc}(y) \approx \frac{1}{6}e^{-y^2} + \frac{1}{2}e^{-\frac{4}{3}y^2}. \tag{26}$$

Thus, one has

$$\begin{aligned} P_{err}^{N} &\approx P_{err,pcsi}^{N,Appr} = \frac{1}{2}D\int_0^{\infty}(I_1 + I_2)X^{MN-1}e^{-X}dX \\ &= \frac{1}{2}D\left(\begin{array}{l}\underbrace{\int_0^{\infty} I_1 X^{MN-1}e^{-X}dX}_{R_1} \\ +\underbrace{\int_0^{\infty} I_2 X^{MN-1}e^{-X}dX}_{R_2}\end{array}\right), \end{aligned} \tag{27}$$

where

$$I_1 = \frac{1}{6}e^{-A^2X+2AB\sqrt{X}-B^2}, \tag{28}$$

$$I_2 = \frac{1}{2}e^{-\frac{4}{3}A^2X+\frac{8}{3}AB\sqrt{X}-\frac{4}{3}B^2}. \tag{29}$$

Let $t = \sqrt{X}$, R_1 can be rewritten as

$$R_1 = \frac{1}{3}e^{-B^2}\int_0^{\infty} e^{\left[-\left(A^2+1\right)t^2+2ABt\right]}t^{2MN-1}dt. \tag{30}$$

Utilizing [63, Eq.(3.462.1)], R_1 can be expressed as

$$\begin{aligned} R_1 = &\frac{1}{3(2A^2+2)^{MN}}\Gamma(2MN)\,e^{\left(\frac{A^2B^2}{2A^2+2}-B^2\right)} \\ &\times \Xi_{-2MN}\left(\frac{-2AB}{\sqrt{2A^2+2}}\right), \end{aligned} \tag{31}$$

where $\Xi_{y_1}(y_2)$ is the parabolic cylinder function, defined as

$$\Xi_{y_1}(y_2) = 2^{\frac{y_2}{2}}e^{-\frac{y_2^2}{4}}\left[\begin{array}{c}\frac{\sqrt{\pi}}{\Gamma\left(\frac{1-y_1}{2}\right)}\cdot{}_1F_1\left(-\frac{y_1}{2},\frac{1}{2};\frac{y_2^2}{2}\right) \\ -\frac{\sqrt{2\pi}y_2}{\Gamma\left(-\frac{y_1}{2}\right)}\cdot{}_1F_1\left(-\frac{1-y_1}{2},\frac{3}{2};\frac{y_2^2}{2}\right)\end{array}\right], \tag{32}$$

and ${}_1F_1(\cdot,\cdot;\cdot)$ is the confluent hypergeometric function [63]. Similarly, R_2 can be expressed by

$$\begin{aligned} R_2 = &\left(\frac{8}{3}A^2+2\right)^{-MN}\Gamma(2MN)\,e^{\left(\frac{8A^2B^2}{12A^2+9}-B^2\right)} \\ &\times \Xi_{-2MN}\left(\frac{-8AB}{\sqrt{24A^2+18}}\right). \end{aligned} \tag{33}$$

Finally, combining Eqs. (27), (31), and (33), the closed-form approximate average BER expression of the proposed STBC-MIMO LoRa system in the perfect scenario is obtained as

$$P_{b,pcsi} \approx \frac{2^{SF-1}}{2^{SF}-1}\cdot P_{err,pcsi}^{N,Appr}. \tag{34}$$

B. Imperfect CSI

In the imperfect CSI scenario, the foregoing approximation method for the Q-function is not utilized in the derivation due to accuracy problem.[7] To obtain the closed-form expression for Eq. (23) in the imperfect scenario, the Gaussian-Hermite quadrature approach [69] is utilized to evaluate P_{err}^{N}, which can be expressed as

$$\int_{-\infty}^{+\infty} f(\xi)d\xi = \sum_{\vartheta=1}^{\rho}\omega_\vartheta f(\xi_\vartheta)e^{\xi_\vartheta^2} + O_\rho, \tag{35}$$

where ρ is the number of samples and it determines the accuracy of the approximation, ξ_ϑ is the ϑ^{th} zero point of the Hermite polynomial, and O_ρ is the remaining term (when ρ approaches infinity, O_ρ decreases to 0), and ω_ϑ is the ϑ^{th} associated weight written as

$$\omega_\vartheta = \frac{2^\rho\rho!\sqrt{\pi}}{\rho^2\Omega_{\rho-1}^2(\xi_\vartheta)}. \tag{36}$$

To solve the integral in P_{err}^{N}, some mathematical processing needs to be performed first. Utilizing variable substitution $\xi = \ln(X)$, P_{err}^{N} can be rewritten as

$$P_{err}^{N} = D\int_{-\infty}^{+\infty} Q\left(\frac{A\sqrt{e^\xi}-B}{C}\right)\cdot e^{\left(MN\xi+Ee^\xi\right)}d\xi. \tag{37}$$

Therefore, by utilizing the Gaussian-Hermite approach given in Eq. (35), P_{err}^{N} in Eq. (23) can be approximated as

$$P_{err,icsi}^{N,Appr} \approx D\cdot\sum_{\vartheta=1}^{\rho}\omega_\vartheta Q\left(\frac{A\sqrt{e^{\xi}}-B}{C}\right)\cdot e^{\left(\xi_\vartheta^2+MN\xi_\vartheta+Ee^{\xi_\vartheta}\right)}. \tag{38}$$

Next, we focus on the derivation of the IAI-driven error probability as follow

$$\begin{aligned} P_{err}^{IAI} = &\int_0^{\infty}\int_0^{\infty}\left[1-\left[1-e^{\frac{-\alpha^2}{2\sigma_\beta^2}}\right]^{J-1}\right] \\ &\times\frac{\alpha}{\sigma_\alpha^2}I_0\left(\frac{m_\alpha\alpha}{\sigma_\alpha^2}\right)e^{\frac{-\left(\alpha^2+m_\alpha^2\right)}{2\sigma_\alpha^2}} \\ &\cdot DX^{(MN-1)}\times e^{EX}d\alpha dX \\ = &D\cdot\int_0^{\infty}\int_0^{\infty}\sum_{\ell=1}^{J-1}(-1)^{\ell+1}\binom{J-1}{\ell}\cdot e^{\frac{-\ell\alpha^2}{2\sigma_\beta^2}} \\ &\times\frac{\alpha}{\sigma_\alpha^2}I_0\left(\frac{m_\alpha\alpha}{\sigma_\alpha^2}\right)\cdot e^{\frac{-\left(\alpha^2+m_\alpha^2\right)}{2\sigma_\alpha^2}} \\ &\cdot X^{(MN-1)}\cdot e^{EX}d\alpha dX, \end{aligned} \tag{39}$$

where $I_\eta(\cdot)$ is η^{th}-order modified Bessel function of the first kind [63] and $\binom{R_1}{R_2} = \frac{R_1!}{R_2!(R_1-R_2)!}$. Owing to $\sigma_\alpha^2 = \sigma_\beta^2$,

[7] In the imperfect CSI scenario, the BER performance of the proposed system in low and middle SNR regions mainly depends on P_{err}^{N}. However, the exponential function based approximation method is usually not very accurate in low or middle SNR regions [59], [61].

Eq. (39) becomes

$$P_{err}^{IAI} = D \cdot \sum_{\ell=1}^{J-1} (-1)^{\ell} \binom{J-1}{\ell} \cdot e^{-\frac{\ell m_\alpha^2}{2(\ell+1)\sigma_\alpha^2}} \times \int_0^\infty \int_0^\infty \frac{\alpha}{\sigma_\alpha^2} I_0\left(\frac{m_\alpha \alpha}{\sigma_\alpha^2}\right) \cdot e^{-\frac{(\ell+1)\alpha^2 + \frac{m_\alpha^2}{(\ell+1)}}{2\sigma_\alpha^2}} \times X^{(MN-1)} \cdot e^{EX} d\alpha dX. \quad (40)$$

By introducing substitutions of variables ${m'}_\alpha = \frac{m_\alpha}{\sqrt{\ell+1}}$ and $\alpha' = \alpha\sqrt{\ell+1}$, Eq. (40) can be rewritten as [29], [61]

$$\begin{aligned} P_{err}^{IAI} &= D \cdot \sum_{\ell=1}^{J-1} (-1)^{\ell+1} \binom{J-1}{\ell} \cdot e^{-\frac{\ell m_\alpha^2}{2(\ell+1)\sigma_\alpha^2}} \times \frac{1}{\ell+1} \int_0^\infty \int_0^\infty \frac{\alpha'}{\sigma_\alpha^2} I_0\left(\frac{\alpha' {m'}_\alpha}{\sigma_\alpha^2}\right) \cdot e^{-\frac{{\alpha'}^2 + {m'}_\alpha{}^2}{2\sigma_\alpha^2}} \times X^{(MN-1)} \cdot e^{EX} d\alpha dX \\ &= D \cdot \sum_{\ell=1}^{J-1} \frac{(-1)^{\ell+1}}{\ell+1} \binom{J-1}{\ell} \times \int_0^\infty e^{-\left(\frac{\ell}{\ell+1} \cdot \frac{\mathrm{T} \cdot 2^{SF}}{\sigma_e^2 \cdot \mathrm{T} \cdot 2^{SF} + rM} - E\right) X} \cdot X^{(MN-1)} dX, \end{aligned} \quad (41)$$

Then, utilizing [63, Eq.(3.351)], a closed-form expression of P_{err}^{IAI} is given by

$$P_{err,clo.}^{IAI} = D \cdot \sum_{\ell=1}^{J-1} \frac{(-1)^{\ell+1}}{\ell+1} \binom{J-1}{\ell} (MN-1)! \times \left(\frac{\ell}{\ell+1} \cdot \frac{\mathrm{T} \cdot 2^{SF}}{\sigma_e^2 \cdot \mathrm{T} \cdot 2^{SF} + rM} - E\right)^{-MN}. \quad (42)$$

Finally, combining Eqs. (16), (38), and (42), the closed-form approximated average BER expression of the proposed STBC-MIMO LoRa system in the imperfect CSI scenario can be expressed as

$$P_{b,icsi} \approx \frac{2^{SF-1}}{2^{SF}-1} \left[P_{err,icsi}^{N,Appr} + \left(1 - P_{err,icsi}^{N,Appr}\right) \times P_{err,clo.}^{IAI}\right]. \quad (43)$$

C. Analysis of Diversity Order

In this subsection, for gaining more insights from the BER analysis, we analyze the diversity order of the proposed STBC-MIMO LoRa system.[8] When $\mathrm{T} \to \infty$, R_1 and R_2 can be approximated as

$$\begin{aligned} R_1 &\approx \frac{1}{3}\Gamma(2MN)\, e^{-\frac{B^2}{2}} \Xi_{-2MN}\left(-\frac{2B}{\sqrt{2}}\right) \times \left(\frac{2^{SF+1}}{rM}\right)^{-MN} \cdot \mathrm{T}^{-MN} \\ &\approx C_1 \cdot \mathrm{T}^{-MN}, \end{aligned} \quad (44)$$

[8]According to [70], the diversity order of the proposed STBC-MIMO LoRa system depends only on the behavior of the PDF $f_X(X)$ around the origin $X = 0$. In the derivation of the approximate average BER expression, we utilize the exact $f_X(X)$ rather than the approximation of $f_X(X)$. Hence, the diversity analysis based on the approximate BER expression can still characterize the behavior of $f_X(X)$.

$$\begin{aligned} R_2 &\approx \Gamma(2MN)\, e^{-\frac{B^2}{3}} \Xi_{-2MN}\left(-\frac{4B}{\sqrt{6}}\right) \times \left(\frac{2^{SF+3}}{3rM}\right)^{-MN} \cdot \mathrm{T}^{-MN} \\ &\approx C_2 \cdot \mathrm{T}^{-MN}. \end{aligned} \quad (45)$$

Thus, combining Eqs. (27), (44), and (45), $P_{b,pcsi}$ can be written as

$$P_{b,pcsi} \approx \frac{1}{2} D\,(C_1 + C_2)\,\mathrm{T}^{-MN}. \quad (46)$$

From expression (46), we can conclude that the diversity order of the proposed system in the perfect CSI scenario is $d = MN$.

Next, we study the diversity order of the STBC-MIMO LoRa system in the imperfect CSI scenario. In this scenario, $P_{b,icsi}$ can be expressed in terms of P_{err}^{N} and $P_{err,clo.}^{IAI}$. For the CEEM I, when T approaches to infinity, $P_{err,icsi}^{N}$ and $P_{err,icsi}^{IAI}$ are approximately expressed respectively as

$$\begin{aligned} P_{err,icsi}^{N} &\approx P_{err,icsi,s}^{N} = \frac{1}{\Gamma(MN)\,(1+\sigma_e^2)^{MN}} \times \int_0^\infty Q\left(\frac{2}{\sigma_e^2} \cdot X\right) X^{MN-1} e^{-\frac{X}{1+\sigma_e^2}} dX, \quad (47) \\ P_{err,icsi}^{IAI} &\approx P_{err,icsi,s}^{IAI} = D \cdot \sum_{\ell}^{J-1} \frac{(-1)^{\ell+1}}{\ell+1} \cdot \binom{J-1}{\ell} \cdot (MN-1)! \times \left(\frac{\ell}{\ell+1} \cdot \frac{1}{\sigma_e^2} - E\right)^{-MN}. \quad (48) \end{aligned}$$

To solve the integral in Eq. (47), the following integral function can be employed [67, Eq. (5A.4a), (5A.4b)]

$$\int_0^\infty Q\left(\sqrt{\varpi x}\right) x^{\varphi-1} e^{-\frac{x}{\varsigma}} dx = \frac{1}{2}\varsigma^{\varphi}\Gamma(\varphi) \times \left(\frac{1-\mu}{2}\right)^{\varphi} \sum_{k=0}^{\varphi-1} \binom{\varphi-1+k}{k} \left(\frac{1+\mu}{2}\right)^{k}, \quad (49)$$

where $\mu = \sqrt{(\varpi\varsigma)/(2+\varpi\varsigma)}$. Then, $P_{err,icsi,s}^{N}$ can be rewritten as

$$P_{err,icsi,s}^{N} = \frac{1}{2}\left[\left(\frac{1-\mu_1}{2}\right)^{MN} \sum_{k=0}^{MN-1} \binom{MN-1+k}{k} \left(\frac{1+\mu_1}{2}\right)^{k}\right], \quad (50)$$

where $\mu_1 = \sqrt{(1+\sigma_e^2)/(1+2\sigma_e^2)}$. Since both $P_{err,icsi,s}^{N}$ and $P_{err,icsi,s}^{IAI}$ are constants, for CEEM I, the diversity order of the STBC-MIMO LoRa system is zero. Therefore, the error floor of BER appears in high SNR region, and one can get the expression of error floor, given by

$$P_{err\_flo.} = \frac{2^{SF-1}}{2^{SF}-1} \cdot \left[P_{err,icsi,s}^{N} + \left(1 - P_{err,icsi,s}^{N}\right) \times P_{err,icsi,s}^{IAI}\right]. \quad (51)$$

According to Eq. (51), the error floor depends on parameters $\left\{M, N, \sigma_e^2\right\}$. For the CEEM II, as T trends to infinity, σ_e^2

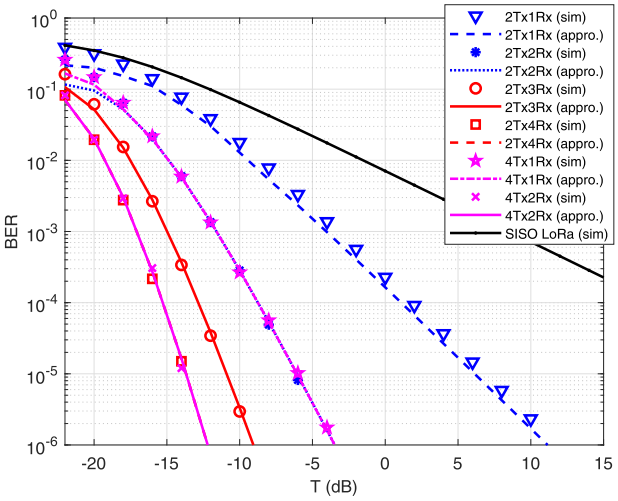

Fig. 3. Simulated and approximated BER results of the proposed STBC-MIMO LoRa system in the perfect CSI scenario. The simulated BER performance of the SISO LoRa system is shown with black solid line.

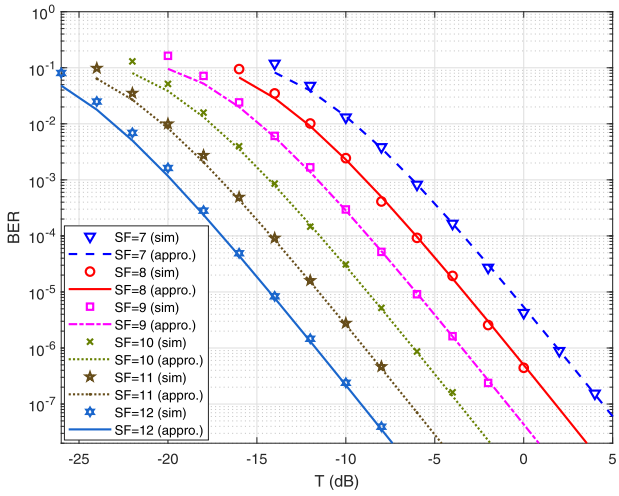

Fig. 4. Simulated and approximate BER results of the proposed STBC-MIMO LoRa system with 4Tx and 1Rx at different spreading factors in the perfect CSI scenario.

becomes zero. Hence, the diversity order of the proposed system for the CEEM II is the same as that in the perfect CSI scenario, which is verified by simulations.

D. Throughput

In a wireless communication system, the throughput is defined as the number of bits that correctly detected by the receiver, which can be expressed as [71]

$$\Upsilon = \frac{F_{pa} N_{bit} \left(1 - P_{pa}\right)}{T_t}, \tag{52}$$

where F_{pa} is the number of the symbols in each packet, $N_{bit} = SF$ is the number of bits in each symbol, T_t is the transmission time per packet, and P_{pa} is the packet error rate, which can be expressed as

$$P_{pa} = 1 - \left(1 - P_s\right)^{F_{pa}}, \tag{53}$$

where $P_s = \frac{2^{SF}-1}{2^{SF-1}} P_{b,\Theta}$ $(\Theta \in \{icsi, pcsi\})$ is the symbol error rate of the proposed system. Moreover, $T_t = \frac{F_{pa} T_c \cdot 2^{SF}}{r}$ and $T_t = F_{pa} T_c \cdot 2^{SF}$ for the proposed system and the SISO LoRa system, respectively. Without loss of generality, we set $T_c = 1$.

IV. Simulation Results and Discussions

In this section, the performance of the proposed STBC-MIMO LoRa system with different space-time codes over a quasi-static flat Rayleigh fading channel is evaluated by simulations, and the simulation results are compared with the theoretical BER performance analysis results to verify the analysis in Sect. III. In addition, $\mathcal{V}$Tx and $\mathcal{Y}$Rx denote $\mathcal{V}$ transmit antennas and $\mathcal{Y}$ receive antennas, respectively. In the following simulations, STBCs $\mathbf{G}_2$ and $\mathbf{G}_4$ in [58] are employed for the system with 2Tx and 4Tx, respectively. Correspondingly, the code rates of 2Tx and 4Tx are 1 and 0.5, respectively. All numerical results and simulation results in this section are obtained utilizing MATLAB. A total of 10^9 Monte Carlo trials were performed to generate the BER curve.

In Fig. 3, we plot the approximate average BER curves and simulation results in the perfect CSI scenario, where SF is set to 9. From Fig. 3, the derived approximate BER results can well match with the simulated ones. Then, it can be seen from these figure that utilizing the STBC-MIMO scheme can significantly improve the diversity gain of the LoRa system. From the perspective of BER performance, taking the STBC-MIMO LoRa system with 2Tx1Rx as an instance, at a BER of 10^{-4}, the proposed system has a 16-dB gain compared to the SISO system. In addition, it can be observed that the STBC-MIMO LoRa systems with 2Tx2Rx and 4Tx1Rx have the same BER performance in the perfect CSI scenario. However, the throughput performance of the STBC-MIMO LoRa systems with these two configurations is different, and the corresponding simulation results are shown later. Similarly, the relative performance between the STBC-MIMO LoRa systems with 2Tx4Rx and 4Tx2Rx, remain the same.

Fig. 4 presents the simulated and approximate BER results of the proposed STBC-MIMO LoRa system with 4Tx and 1Rx for all possible spreading factors $SF \in \{7, \ldots, 12\}$ in the perfect CSI scenario. It can be seen from the figure that the simulated results are consistent with the approximate ones. In addition, BER performance increases with the increase of SF. This law in the STBC-MIMO LoRa system is consistent with that in the SISO LoRa system [18].

Furthermore, two different channel estimation error models are utilized to evaluate the proposed STBC-MIMO LoRa system with imperfect CSI, i.e., CEEM I (σ_e^2 is fixed) and CEEM II ($\sigma_e^2 = 1/\left(1 + L_p \mathrm{T}_{eff}\right)$). L_p is set to 4. The simulated and approximate BER results of the proposed STBC-MIMO LoRa system in the imperfect CSI scenario with CEEM I are shown in Fig. 5. From this figure, it is observed that in the proposed system with the same number of the transmit and receive antenna, the error floor becomes higher as σ_e^2 increases. For a fixed σ_e^2, increasing the number of the transmit or receive antenna can reduce the error floor.

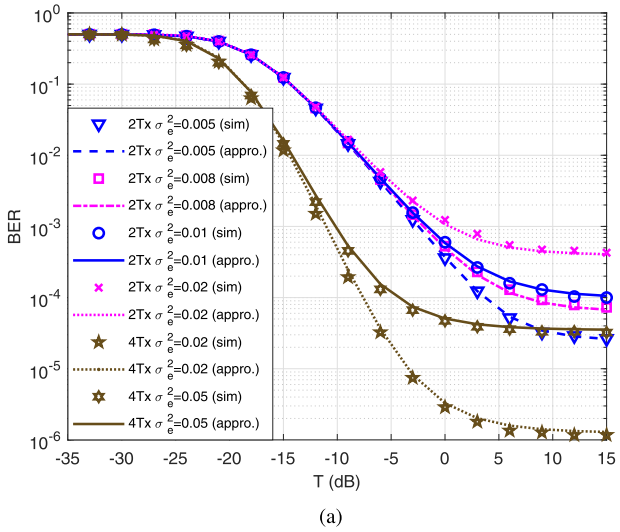

(a)

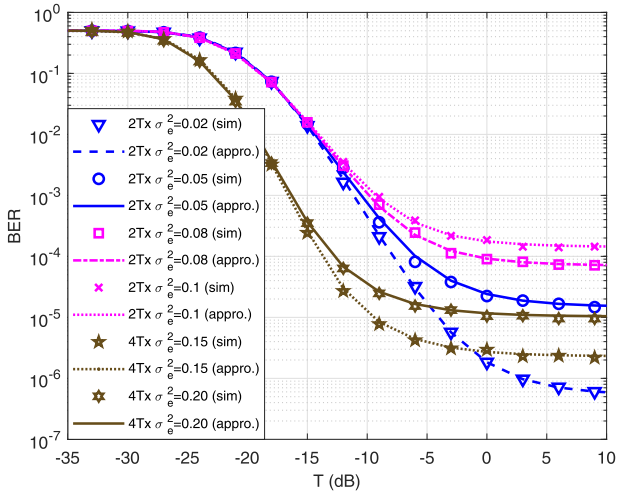

(b)

Fig. 5. Simulated and approximate BER results of the proposed STBC-MIMO LoRa system with (a)1Rx and (b)2Rx in the imperfect CSI scenario (CEEM I).

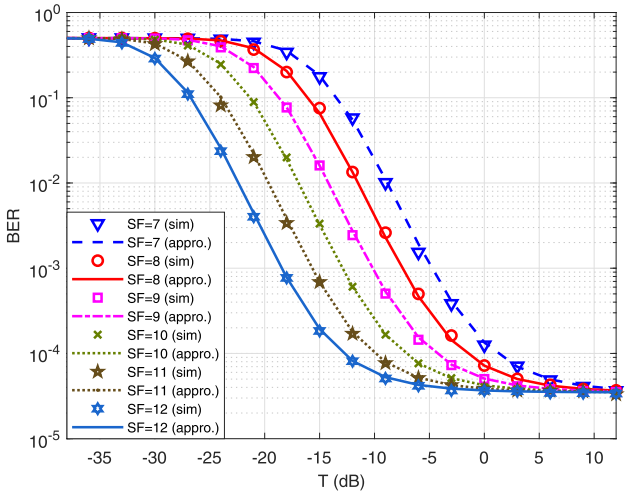

Fig. 6. Simulated and approximate BER results of the proposed STBC-MIMO LoRa system with 4Tx and 1Rx in the imperfect CSI scenario (CEEM I) at different spreading factors, where $\sigma_e^2 = 0.05$.

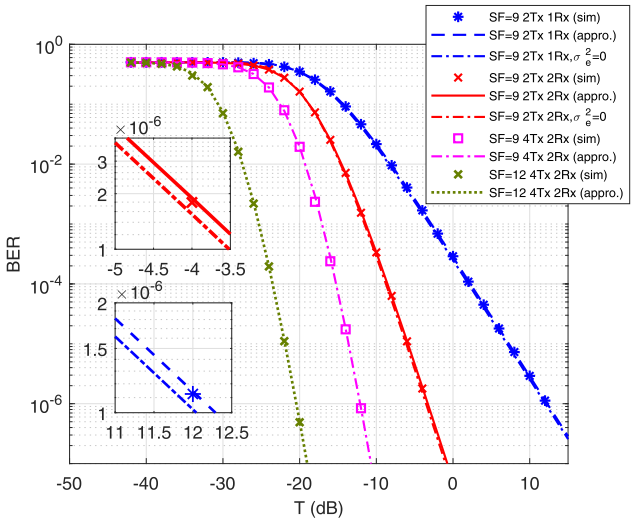

Fig. 7. Simulated and approximate BER results of the proposed STBC-MIMO LoRa system in the imperfect CSI scenario (CEEM II).

Fig. 6 presents the simulated and approximate BER results of the proposed STBC-MIMO LoRa system with 4Tx and 1Rx at different spreading factors in the imperfect CSI scenario with CEEM I, where $SF \in \{7, \ldots 12\}$ and $\sigma_e^2 = 0.05$. As expected, for an STBC-MIMO LoRa systems with the same parameters $\{M, N, \sigma_e^2\}$, the change of SF does not affect the error floor of the BER. Then, Fig. 5 and Fig. 6 not only verify the accuracy of the derived approximate BER in the imperfect CSI scenario, but also show that the diversity order of the proposed STBC-MIMO LoRa system is zero under the CEEM I.

Fig. 7 shows the simulated and approximate BER results of the proposed STBC-MIMO LoRa system in the imperfect CSI scenario with CEEM II (i.e., σ_e^2 is a decreasing function of SNR). It can be seen from this figure that under the CEEM II, the diversity order of the proposed system is the same as that in the perfect CSI scenario, which verifies the conclusion obtained by the analysis of the diversity order in Sect. III-C. In high SNR region, BER performance of the proposed STBC-MIMO LoRa system under CEEM II is worse than that under perfect CSI, but the system performance in these two cases is very similar because σ_e^2 is very small in high SNR region. Furthermore, the results also show that the derived approximate BER expression is valid for CEEM II.

Fig. 8 illustrates the throughput of the proposed STBC-MIMO LoRa system and the SISO LoRa system, where F_{pa} is set to 8. In the proposed system, the throughput depends on the SF and STBC utilized. Since the transmission rate of $\mathbf{G}_2$ is twice that of $\mathbf{G}_4$, the throughput of the STBC-MIMO LoRa system with 2Tx2Rx is twice that of the STBC-MIMO LoRa system with 4Tx1Rx at the same SF. Compared to the SISO LoRa system, the STBC-MIMO LoRa system can achieve its maximum throughput at a lower SNR. Taking the STBC-MIMO LoRa system with 2Tx2Rx as an example, the SNR required by the system to achieve its maximum throughput is about 24 dB lower than that of the SISO LoRa

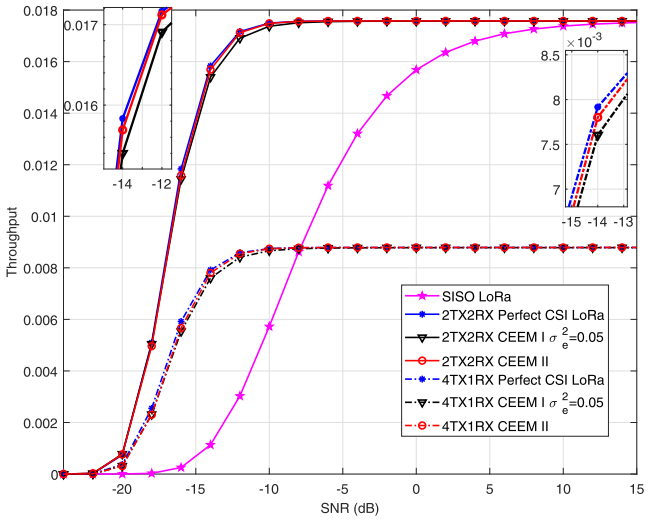

Fig. 8. Throughput of the STBC-MIMO LoRa system and the SISO LoRa system, SF is set to 9.

system. Moreover, in the middle SNR region, we observe that the throughput in the perfect CSI scenario is slightly higher than that in the imperfect CSI scenario for the STBC-MIMO LoRa systems with the same parameters. In the high SNR region, the STBC-MIMO LoRa system has almost the same throughput under different CSI conditions.

Based on the results of theoretical analysis and simulation, we can obtain some design insight for the proposed STBC-MIMO LoRa system. For LoRa-based LPWAN, in the entire transmission duration after LoRa node connect with the LoRa gateway, the uplink transmission occupies most of the time (e.g., class A of LoRaWAN protocol [14], [52]). This is because the main role of LoRa based LPWAN is to transmit the data of the LoRa nodes to the LoRa gateway. Therefore, how to transmit more data within the precious uplink transmission duration is particularly important. Considering the low power and low complexity requirements of LoRa nodes and the throughput performance of the system, equipping LoRa nodes with two antennas and utilizing $\mathbf{G}_2$ for transmission could be considered as an efficient solution (for complex STBC, only Alamouti code $\mathbf{G}_2$ can achieve $r = 1$ [36]). In order to further improve the reliability of the system, more antennas can be equipped at the LoRa gateway to achieve higher diversity and reduce the impact of channel estimation error (see Fig. 5). Although this configuration will increase the hardware complexity and computational complexity of the LoRa gateway (refer to Sect. II-C), the LoRa gateway is generally not sensitive to the complexity and energy consumption in practice.

V. Conclusion

In this paper, an STBC-MIMO LoRa system has been presented and its theoretical performance has been carefully studied. To be specific, the closed-form approximate BER expression of the proposed STBC-MIMO LoRa system for the perfect and imperfect CSI scenarios has been derived. As a further advance, the diversity order of the proposed system has been analyzed. According to the analyzed results, the diversity order of the proposed system is zero in the imperfect CSI scenario with CEEM I, hence the error floor appears in high SNR region. In addition, full-diversity order $d = MN$ can be achieved in the imperfect CSI scenario with CEEM II and the perfect CSI scenario. Afterward, the throughput analysis demonstrates that the STBC-MIMO LoRa system with the same parameters has almost the same throughput under different CSI conditions. Simulated BER results not only are in well agreement with the theoretical ones, but also verify the excellent performance and potential of the proposed STBC-MIMO LoRa system. From the perspective of BER performance, throughput, and complexity, configuring two antennas for the LoRa node and more antennas for the LoRa gateway can be regarded as an efficient solution in LoRa based LPWAN. Hence, the proposed system can be considered as a promising scheme for LPWAN.

References

[1] M. R. Palattella *et al.*, "Internet of Things in the 5G era: Enablers, architecture, and business models," *IEEE J. Sel. Areas Commun.*, vol. 34, no. 3, pp. 510–527, Mar. 2016.
[2] C. Bernier, F. Dehmas, and N. Deparis, "Low complexity LoRa frame synchronization for ultra-low power software-defined radios," *IEEE Trans. Commun.*, vol. 68, no. 5, pp. 3140–3152, May 2020.
[3] A. Hoglund *et al.*, "Overview of 3GPP release 14 enhanced NB-IoT," *IEEE Netw.*, vol. 31, no. 6, pp. 16–22, Nov./Dec. 2017.
[4] M. Lauridsen, B. Vejlgaard, I. Z. Kovacs, H. Nguyen, and P. Mogensen, "Interference measurements in the European 868 MHz ISM band with focus on LoRa and SigFox," in *Proc. IEEE Wireless Commun. Netw. Conf. (WCNC)*, Mar. 2017, pp. 1–6.
[5] J.-T. Lim and Y. Han, "Spreading factor allocation for massive connectivity in LoRa systems," *IEEE Commun. Lett.*, vol. 22, no. 4, pp. 800–803, Apr. 2018.
[6] U. Raza, P. Kulkarni, and M. Sooriyabandara, "Low power wide area networks: An overview," *IEEE Commun. Surveys Tuts.*, vol. 19, no. 2, pp. 855–873, 2nd Quart., 2017.
[7] D. Croce, M. Gucciardo, S. Mangione, G. Santaromita, and I. Tinnirello, "LoRa technology demystified: From link behavior to cell-level performance," *IEEE Trans. Wireless Commun.*, vol. 19, no. 2, pp. 822–834, Feb. 2020.
[8] L. Vangelista, "Frequency shift chirp modulation: The LoRa modulation," *IEEE Signal Process. Lett.*, vol. 24, no. 12, pp. 1818–1821, Dec. 2017.
[9] T. Elshabrawy and J. Robert, "Capacity planning of LoRa networks with joint noise-limited and interference-limited coverage considerations," *IEEE Sensors J.*, vol. 19, no. 11, pp. 4340–4348, Jun. 2019.
[10] S.-Y. Wang *et al.*, "Performance of LoRa-based IoT applications on campus," in *Proc. IEEE 86th Veh. Technol. Conf. (VTC-Fall)*, Sep. 2017, pp. 1–6.
[11] O. Georgiou and U. Raza, "Low power wide area network analysis: Can LoRa scale?" *IEEE Wireless Commun. Lett.*, vol. 6, no. 2, pp. 162–165, Apr. 2017.
[12] K. E. Nolan, W. Guibene, and M. Y. Kelly, "An evaluation of low power wide area network technologies for the Internet of Things," in *Proc. Int. Wireless Commun. Mobile Comput. Conf. (IWCMC)*, Sep. 2016, pp. 439–444.
[13] J. Petajajarvi, K. Mikhaylov, A. Roivainen, T. Hanninen, and M. Pettissalo, "On the coverage of LPWANs: Range evaluation and channel attenuation model for LoRa technology," in *Proc. 14th Int. Conf. ITS Telecommun. (ITST)*, Dec. 2015, pp. 55–59.
[14] D. Bankov, E. Khorov, and A. Lyakhov, "Mathematical model of LoRaWAN channel access," in *Proc. IEEE 18th Int. Symp. World Wireless, Mobile Multimedia Netw. (WoWMoM)*, Jun. 2017, pp. 1–3.
[15] F. Van den Abeele, J. Haxhibeqiri, I. Moerman, and J. Hoebeke, "Scalability analysis of large-scale LoRaWAN networks in ns-3," *IEEE Internet Things J.*, vol. 4, no. 6, pp. 2186–2198, Dec. 2017.
[16] A. Augustin, J. Yi, C. Thomas, and T. William, "A study of LoRa: Long range & low power networks for the Internet of Things," *Sensors*, vol. 16, no. 9, pp. 1466–1483, Sep. 2016.

[17] K. Mikhaylov, J. Petaejaejaervi, and T. Haenninen, "Analysis of capacity and scalability of the LoRa low power wide area network technology," in *Proc. Eur. Wireless Conf. (EW)*, Dec. 2016, pp. 1–6.

[18] O. Afisiadis, M. Cotting, A. Burg, and A. Balatsoukas-Stimming, "On the error rate of the LoRa modulation with interference," *IEEE Trans. Wireless Commun.*, vol. 19, no. 2, pp. 1292–1304, Feb. 2020.

[19] R. Fernandes, R. Oliveira, M. Luís, and S. Sargento, "On the real capacity of LoRa networks: The impact of non-destructive communications," *IEEE Commun. Lett.*, vol. 23, no. 12, pp. 2437–2441, Dec. 2019.

[20] C.-H. Liao, G. Zhu, D. Kuwabara, M. Suzuki, and H. Morikawa, "Multi-hop LoRa networks enabled by concurrent transmission," *IEEE Access*, vol. 5, pp. 21430–21446, 2017.

[21] G. Zhu, C.-H. Liao, T. Sakdejayont, I.-W. Lai, Y. Narusue, and H. Morikawa, "Improving the capacity of a mesh LoRa network by spreading-factor-based network clustering," *IEEE Access*, vol. 7, pp. 21584–21596, 2019.

[22] P. Branch and T. Cricenti, "A LoRa based wireless relay network for actuator data," in *Proc. Int. Conf. Inf. Netw. (ICOIN)*, Jan. 2020, pp. 190–195.

[23] S. S. Borkotoky, U. Schilcher, and C. Bettstetter, "Cooperative relaying in LoRa sensor networks," in *Proc. IEEE Global Commun. Conf. (GLOBECOM)*, Dec. 2019, pp. 1–5.

[24] O. B. Seller and N. Sornin, "Low power long range transmitter," U.S. Patent 47 720 329, Aug. 7, 2014.

[25] M. Knight and B. Seeber, "Decoding LoRa: Realizing a modern LPWAN with SDR," in *Proc. GNU Radio Conf.*, Sep. 2016, vol. 1, no. 1, pp. 1–5.

[26] P. Robyns, P. Quax, W. Lamotte, and W. Thenaers, "A multi-channel software decoder for the LoRa modulation scheme," in *Proc. 3rd Int. Conf. Internet Things, Big Data Secur. (IoTBDS)*, 2018, pp. 41–51.

[27] M. Chiani and A. Elzanaty, "On the LoRa modulation for IoT: Waveform properties and spectral analysis," *IEEE Internet Things J.*, vol. 6, no. 5, pp. 8463–8470, Oct. 2019.

[28] T. Elshabrawy and J. Robert, "Closed-form approximation of LoRa modulation BER performance," *IEEE Commun. Lett.*, vol. 22, no. 9, pp. 1778–1781, Sep. 2018.

[29] C. F. Dias, E. R. de Lima, and G. Fraidenraich, "Bit error rate closed-form expressions for LoRa systems under nakagami and rice fading channels," *Sensors*, vol. 19, no. 20, p. 4412, Oct. 2019.

[30] R. Bomfin, M. Chafii, and G. Fettweis, "A novel modulation for IoT: PSK-LoRa," in *Proc. IEEE 89th Veh. Technol. Conf. (VTC-Spring)*, Apr. 2019, pp. 1–5.

[31] T. Elshabrawy and J. Robert, "Interleaved chirp spreading LoRa-based modulation," *IEEE Internet Things J.*, vol. 6, no. 2, pp. 3855–3863, Apr. 2019.

[32] L. Vangelista and A. Cattapan, "A new LoRa-compatible modulation improving the LoRaWAN network level performance," in *Proc. IEEE Latin-Amer. Conf. Commun. (LATINCOM)*, Nov. 2019, pp. 1–6.

[33] A. R. Flores, R. C. De Lamare, and B. Clerckx, "Tomlinson-Harashima precoded rate-splitting with stream combiners for MU-MIMO systems," *IEEE Trans. Commun.*, early access, Mar. 10, 2021, doi: 10.1109/TCOMM.2021.3065145.

[34] S. M. Alamouti, "A simple transmit diversity technique for wireless communications," *IEEE J. Sel. Areas Commun.*, vol. 16, no. 8, pp. 1451–1458, Oct. 1998.

[35] V. Tarokh, H. Jafarkhani, and A. R. Calderbank, "The application of orthogonal designs to wireless communication," in *Proc. IEEE Inf. Theory Workshop*, Jun. 1998, pp. 46–47.

[36] V. Tarokh, H. Jafarkhani, and A. R. Calderbank, "Space-time block codes from orthogonal designs," *IEEE Trans. Inf. Theory*, vol. 45, no. 5, pp. 1456–1467, Jul. 1999.

[37] J.-C. Belfiore, G. Rekaya, and E. Viterbo, "The golden code: A 2×2 full-rate space-time code with nonvanishing determinants," *IEEE Trans. Inf. Theory*, vol. 51, no. 4, pp. 1432–1436, Apr. 2005.

[38] B. Sirkeci-Mergen and A. Scaglione, "Randomized space-time coding for distributed cooperative communication," *IEEE Trans. Signal Process.*, vol. 55, no. 10, pp. 5003–5017, Oct. 2007.

[39] T. Peng, R. C. de Lamare, and A. Schmeink, "Adaptive distributed space-time coding based on adjustable code matrices for cooperative MIMO relaying systems," *IEEE Trans. Commun.*, vol. 61, no. 7, pp. 2692–2703, Jul. 2013.

[40] R. De Lamare and R. Sampaio-Neto, "Blind adaptive MIMO receivers for space-time block-coded DS-CDMA systems in multipath channels using the constant modulus criterion," *IEEE Trans. Commun.*, vol. 58, no. 1, pp. 21–27, Jan. 2010.

[41] D. Reynolds, X. Wang, and H. V. Poor, "Blind adaptive space-time multiuser detection with multiple transmitter and receiver antennas," *IEEE Trans. Signal Process.*, vol. 50, no. 6, pp. 1261–1276, Jun. 2002.

[42] H. C. Hwang and K. S. Kwak, "Space-time MMSE multiuser receiver for space-time coded DS/CDMA systems in frequency selective fading channels," in *Proc. IEEE Veh. Technol. Conf. (VTC)*, Apr. 2003, pp. 759–763.

[43] F. Petre, G. Leus, L. Deneire, M. Engels, M. Moonen, and H. De Man, "Space-time block coding for single-carrier block transmission DS-CDMA downlink," *IEEE J. Sel. Areas Commun.*, vol. 21, no. 3, pp. 350–361, Apr. 2003.

[44] J. Xu, P. Zhang, S. Zhong, and L. Huang, "Discrete particle swarm optimization based antenna selection for MIMO LoRa IoT systems," in *Proc. Comput., Commun. IoT Appl. (ComComAp)*, Oct. 2019, pp. 204–209.

[45] M. N. Mahfoudi, G. Sivadoss, O. B. Koachi, T. Turletti, and W. Dabbous, "Joint range extension and localization for LPWAN," *Internet Technol. Lett.*, vol. 2, no. 5, p. e120, Sep./Oct. 2019.

[46] M. N. Mahfoudi, O. B. Koachi, G. Sivadoss, T. Turletti, W. Dabbous, L. Lizzi, and F. Ferrero. *MIMO-Based Range Extension for LP-WAN*. Accessed: Mar. 4, 2019. [Online]. Available: https://ds4h.univ-cotedazur.eu/medias/fichier/190403-dabbous_1594647505660-pdf?ID_FICHE=21940&INLINE=FALSE

[47] J. R. Magnus and H. Neudecker, *Matrix Differential Calculus With Applications in Statistics and Econometrics*. Hoboken, NJ, USA: Wiley, 1988.

[48] D. Wen, G. Zhu, and K. Huang, "Reduced-dimension design of MIMO over-the-air computing for data aggregation in clustered IoT networks," *IEEE Trans. Wireless Commun.*, vol. 18, no. 11, pp. 5255–5268, Nov. 2019.

[49] Q. Qi, X. Chen, and D. W. K. Ng, "Robust beamforming for NOMA-based cellular massive IoT with SWIPT," *IEEE Trans. Signal Process.*, vol. 68, pp. 211–224, 2020.

[50] P. Chen, Z. Xie, Y. Fang, Z. Chen, S. Mumtaz, and J. J. P. C. Rodrigues, "Physical-layer network coding: An efficient technique for wireless communications," *IEEE Netw.*, vol. 34, no. 2, pp. 270–276, Mar. 2020.

[51] Y. Fang, P. Chen, G. Cai, F. C. M. Lau, S. C. Liew, and G. Han, "Outage-limit-approaching channel coding for future wireless communications: Root-protograph low-density parity-check codes," *IEEE Veh. Technol. Mag.*, vol. 14, no. 2, pp. 85–93, Jun. 2019.

[52] *LoRaWAN Specifications*. Accessed: Oct. 11, 2017. [Online]. Available: https://lora-alliance.org/sites/default/files/2018-04/lorawantm_specification_-v1.1.pdf

[53] H. Shin and H. Lee, "Performance analysis of space-time block codes over keyhole nakagami-m fading channels," *IEEE Trans. Veh. Technol.*, vol. 53, no. 2, pp. 351–362, Mar. 2004.

[54] X. Yu, Y. Rui, X. Yin, and S. H. Leung, "Precoding scheme for space-time-coded multiple-input–multiple-output system with estimation error and feedback delay in Rayleigh fading channel," *IET Commun.*, vol. 6, no. 16, pp. 2525–2533, Nov. 2012.

[55] Q. Li, M. Wen, E. Basar, H. V. Poor, B. Zheng, and F. Chen, "Diversity enhancing multiple-mode OFDM with index modulation," *IEEE Trans. Commun.*, vol. 66, no. 8, pp. 3653–3666, Aug. 2018.

[56] P. Aquilina and T. Ratnarajah, "Linear interference alignment in full-duplex MIMO networks with imperfect CSI," *IEEE Trans. Commun.*, vol. 65, no. 12, pp. 5226–5243, Dec. 2017.

[57] A. E. Canbilen, S. S. Ikki, E. Basar, S. S. Gultekin, and I. Develi, "Joint impact of I/Q imbalance and imperfect CSI on SM-MIMO systems over generalized beckmann fading channels: Optimal detection and Cramér–Rao bound," *IEEE Trans. Wireless Commun.*, vol. 19, no. 5, pp. 3034–3046, May 2020.

[58] V. Tarokh, H. Jafarkhani, and A. R. Calderbank, "Space-time block coding for wireless communications: Performance results," *IEEE J. Sel. Areas Commun.*, vol. 17, no. 3, pp. 451–460, Mar. 1999.

[59] X. Yu, W. Xu, S.-H. Leung, and J. Wang, "Unified performance analysis of transmit antenna selection with OSTBC and imperfect CSI over Nakagami-m fading channels," *IEEE Trans. Veh. Technol.*, vol. 67, no. 1, pp. 494–508, Jan. 2018.

[60] S. J. Lee, "On the training of MIMO-OFDM channels with least square channel estimation and linear interpolation," *IEEE Commun. Lett.*, vol. 12, no. 2, pp. 100–102, Feb. 2008.

[61] J. G. Proakis and M. Salehi, *Digital Communications*, 5th ed. New York, NY, USA: McGraw-Hill, 2007.

[62] T. Elshabrawy and J. Robert, "Analysis of BER and coverage performance of LoRa modulation under same spreading factor interference," in *Proc. IEEE 29th Annu. Int. Symp. Pers., Indoor Mobile Radio Commun. (PIMRC)*, Sep. 2018, pp. 1–6.

[63] I. S. Gradshteyn and I. M. Ryzhik, *Table of Integrals, Series and Products*, 7th ed. Berkeley, CA, USA: Academic, 2007.
[64] W. M. Gifford, M. Z. Win, and M. Chiani, "Diversity with practical channel estimation," *IEEE Trans. Wireless Commun.*, vol. 4, no. 4, pp. 1935–1947, Jul. 2005.
[65] G. Cai, Y. Fang, G. Han, J. Xu, and G. Chen, "Design and analysis of relay-selection strategies for two-way relay network-coded DCSK systems," *IEEE Trans. Veh. Technol.*, vol. 67, no. 2, pp. 1258–1271, Feb. 2018.
[66] G. Cai, Y. Fang, P. Chen, G. Han, G. Cai, and Y. Song, "Design of an MISO-SWIPT-aided code-index modulated multi-carrier M-DCSK system for e-health IoT," *IEEE J. Sel. Areas Commun.*, vol. 39, no. 2, pp. 311–324, Feb. 2020.
[67] M. K. Simon and M. S. Alouini, *Digital Communication Over Fading Channels*, 2nd ed. New York, NY, USA: Wiley, 2005.
[68] M. Chiani, D. Dardari, and M. K. Simon, "New exponential bounds and approximations for the computation of error probability in fading channels," *IEEE Trans. Wireless Commun.*, vol. 24, no. 5, pp. 840–845, May 2003.
[69] M. Abramowitz and I. A. Stegun, *Handbook of Mathematical Functions: With Formulas, Graphs, and Mathematical Tables*. New York, NY, USA: Dover, 1996.
[70] Z. Wang and G. B. Giannakis, "A simple and general parameterization quantifying performance in fading channels," *IEEE Trans. Commun.*, vol. 51, no. 8, pp. 1389–1398, Aug. 2003.
[71] Z. Wang, Q. Peng, and L. B. Milstein, "Multi-user resource allocation for downlink multi-cluster multicarrier DS CDMA system," *IEEE Trans. Wireless Commun.*, vol. 10, no. 8, pp. 2534–2542, Aug. 2011.

Huan Ma received the B.Sc. degree in communication engineering from Heilongjiang University, Harbin, China, in 2017, and the M.Sc. degree in electronic and communication engineering from the Guangdong University of Technology, Guangzhou, China, in 2020, where he is currently pursuing the Ph.D. degree with the Department of Communication Engineering. His research interests include spread-spectrum modulation and the Internet of Things.

Guofa Cai (Member, IEEE) received the B.S. degree in communication engineering from Jimei University, Xiamen, China, in 2007, the M.S. degree in circuits and systems from Fuzhou University, Fuzhou, China, in 2012, and the Ph.D. degree in communication engineering from Xiamen University, Xiamen, in 2015. He was a Research Fellow with the School of Electrical and Electronic Engineering, Nanyang Technological University, Singapore, in 2017. He is currently an Associate Professor with the School of Information Engineering, Guangdong University of Technology, China. His research interests include information theory and coding, spread-spectrum modulation, wireless body area networks, and the Internet of Things.

Yi Fang (Member, IEEE) received the Ph.D. degree in communication engineering from Xiamen University, China, in 2013. From May 2012 to July 2012, he was a Research Assistant in electronic and information engineering with The Hong Kong Polytechnic University, Hong Kong. From September 2012 to September 2013, he was a Visiting Scholar in electronic and electrical engineering with University College London, U.K. From February 2014 to February 2015, he was a Research Fellow with the School of Electrical and Electronic Engineering, Nanyang Technological University, Singapore. He is currently a Full Professor and the Vice Dean of the School of Information Engineering, Guangdong University of Technology, China. His current research interests include information and coding theory, spread-spectrum modulation, and cooperative communications. He served as the Publicity Co-Chair for the International Symposium on Turbo Codes and Iterative Information Processing 2018.

Pingping Chen (Member, IEEE) received the Ph.D. degree in electronic engineering from Xiamen University, China, in 2013. He was a Research Assistant in electronic and information engineering with The Hong Kong Polytechnic University, Hong Kong, in 2012. From 2013 to 2015, he was a Post-Doctoral Fellow with the Institute of Network Coding, The Chinese University of Hong Kong, Hong Kong. He is currently a Full Professor with Fuzhou University, China. His research interests include channel coding, joint source and channel coding, network coding, and UWB communications.

Guojun Han (Senior Member, IEEE) received the M.E. degree in electronic engineering from the South China University of Technology, Guangzhou, China, and the Ph.D. degree from Sun Yat-sen University, Guangzhou. From March 2011 to August 2013, he was a Research Fellow with the School of Electrical and Electronic Engineering, Nanyang Technological University, Singapore. From October 2013 to April 2014, he was a Research Associate with the Department of Electrical and Electronic Engineering, The Hong Kong University of Science and Technology. He is currently a Full Professor and the Executive Dean of the School of Information Engineering, Guangdong University of Technology, Guangzhou. His research interests include wireless communications, and coding and signal processing for data storage.